

RESEARCH ARTICLE

A multi-model analysis of the East Asian monsoon changes in the Medieval Climate Anomaly and Little Ice Age

Kaiqing Yang  | Wei Hua  | Qin Hu 

School of Atmospheric Sciences/Plateau Atmosphere and Environment Key Laboratory of Sichuan Province/Joint Laboratory of Climate and Environment Change, Chengdu University of Information Technology, Chengdu, China

Correspondence

Wei Hua, School of Atmospheric Sciences/Plateau Atmosphere and Environment Key Laboratory of Sichuan Province/Joint Laboratory of Climate and Environment Change, Chengdu University of Information Technology, Chengdu 610225, China.
Email: huawei@cuit.edu.cn

Funding information

National Natural Science Foundation of China, Grant/Award Number: 41775072; Outstanding Young Talents Project of Sichuan Province, Grant/Award Number: 2019JDJQ0001; the National Key R&D Program of China, Grant/Award Number: 2018YFC1505702; the Scientific Research Foundation of Key Laboratory of Meteorological Disaster, Ministry of Education, Grant/Award Number: KLME201803

Abstract

Using nine climate model simulations from the Paleoclimate Modelling Intercomparison Project Phase 3, the changes in the East Asian summer and winter monsoon, together with their associated atmospheric circulations in the Medieval Climate Anomaly (MCA) and Little Ice Age (LIA), were investigated in this study. The East Asian summer monsoon strengthened (weakened) as a consequence of the increased (decreased) land–sea thermal contrast between the East Asian continent and the adjacent western North Pacific and South China Sea in the MCA (LIA). The East Asian winter monsoon (EAWM) changes varied across models, and differences were shown between the low latitudes and mid-to-high latitudes of the EAWM region. In the northern area, the EAWM intensified slightly due to a reinforced Aleutian Low during the MCA and decreased slightly because of the suppression of the Siberian High and the weakening and northward shift of the Aleutian Low during the LIA. In contrast, there are large inconsistencies among models during both periods in the southern EAWM region. Our results imply that model improvement is needed to reproduce the complex interacting processes over the low latitudes of East Asia.

KEYWORDS

East Asian summer monsoon, East Asian winter monsoon, LIA, MCA, model

1 | INTRODUCTION

The East Asian monsoon (EAM), which includes the East Asian summer monsoon (EASM) and East Asian winter monsoon (EAWM), is one of the most important components of Asian climate system. The EAM exerts a direct impact on temperature and precipitation regulation in densely populated East Asia and consequently relates to the occurrence of disasters and extreme events, such as floods, droughts and severe cold/hot events. Much effort has been made to understand the recent and future changes in the EAM over various time scales, and the role of external forcing and natural internal variability has also been addressed (Chen *et al.*, 2000; Jiang and

Wang, 2005; Ding *et al.*, 2008; Wang and Chen, 2010; Jiang and Tian, 2013; Chen *et al.*, 2014). However, instrumental observations only cover the last few decades; in an attempt to better understand the present-day EAM behaviour and conduct future predictions to reduce the damage caused by these disasters, it is necessary to extend the temporal scale into the past.

Geological evidence shows multiple time scale temperature variations over the past millennium. On the centennial scale, there are two widely recognized climate intervals. One interval is the Medieval Climate Anomaly (MCA), which is characterized by warm surface temperature, high solar irradiance and low volcanic activity, and the other interval is the Little Ice Age (LIA), which is

characterized by cold temperature, low solar activity and frequent volcanic eruptions (Mann and Jones, 2003; Juckes *et al.*, 2007; Mann *et al.*, 2009; PAGES 2k Consortium, 2013; Hakim *et al.*, 2016). Reconstruction studies regarding the EASM suggest that East Asia generally experienced a stronger EASM during the MCA than during the LIA (Wang *et al.*, 2005; Hu *et al.*, 2008; Zhang *et al.*, 2008; Li *et al.*, 2017). By comparing the EASM evolution with other proxy data, it is further proposed that external forcing factors such as solar activity (Wang *et al.*, 2005; Zhang *et al.*, 2008; Li *et al.*, 2017) and internal variability modes such as the Asia-Pacific Oscillation (Fang *et al.*, 2014) and Pacific Decadal Oscillation (Lee and Park, 2015; Zhao *et al.*, 2015) may affect the EASM variation. On the other hand, the sequences of the Holocene EAWM are less well established than those of the EASM because of unsuitable archives and proxies (Sagawa *et al.*, 2014), and discrepancies are evident among different reconstruction results (Xiao *et al.*, 2006; Liu *et al.*, 2009; Sagawa *et al.*, 2014; Tu *et al.*, 2017; Li *et al.*, 2018). It is also implied that changes in the Holocene EAWM were likely forced by the reduction in solar irradiance through changes in the oceanic–atmospheric circulation patterns on the centennial scale (Sagawa *et al.*, 2014), and Arctic Sea ice may have modulated the relationship between the EAWM and the Atlantic Oscillation (Li *et al.*, 2018). However, given the sporadic distribution and limited indicators of proxies, the mechanisms behind the EAM variations are incomprehensively interpreted.

Climate models provide an approach for determining the dynamic processes that are responsible for past climate changes; therefore, simulating the EAM over the last millennium is of high interest. Based on different climate models, studies concerning the EASM have consistently showed a strengthened (weakened) EASM during the MCA (LIA) (Peng *et al.*, 2010; Liu *et al.*, 2011; Man *et al.*, 2012; Landrum *et al.*, 2013; Man and Zhou, 2014), and this change tends to closely follow the effective radiation forcing that relates to both solar irradiation and volcanic aerosols (Liu *et al.*, 2011; Man *et al.*, 2012; Landrum *et al.*, 2013; Man and Zhou, 2014). Furthermore, large volcanic eruptions can cause the summer precipitation over eastern China to significantly decrease for a period of 2–3 years and may even trigger drought events in eastern China (Anchukaitis *et al.*, 2010; Peng *et al.*, 2010; Peng *et al.*, 2014). However, it should be noted that the boundary conditions applied by these simulations are obtained from different reconstructions, which leads to uncertainties in directly comparing these results. In addition, most of these studies mainly focused on the EASM, little effort has been made to understand the EAWM.

The Paleoclimate Modelling Intercomparison Project Phase 3 (PMIP3) provides new insights into past climate investigations. Based on multi-model experiments, Shi *et al.* (2016a) addressed the mechanism of the tripole

humidity pattern in the Asian region and implied the effects of the La Niña (El Niño)-like conditions during the last millennium. Shi *et al.* (2016b) compared Asian climate differences between the MCA and LIA and noted overestimated natural forcing impacts on Asian monsoon rainfall. However, the changes in the EAM in multiple climate models are still insufficiently determined, especially for the EAWM. Therefore, in this study, simulations of the last millennium from the PMIP3 are analysed with the aim to examine the EASM and EAWM changes and the underlying physical mechanisms in the non-anthropogenic warm and cold climate backgrounds.

2 | DATA AND METHOD

Eleven climate models have performed the last millennium experiment in the PMIP3. Considering that MIROC-ESM has a long-term climate drift (Sen Gupta *et al.*, 2013) and BCC-CSM1.1 includes unsolvable missing values, the remaining nine models were used in this study. We consider only one (R124, with almost the same boundary conditions as the other models) of the eight GISS-E2-R ensembles (R121–128) to avoid overemphasizing the influence of this model. Basic information of these models is provided in Table 1, and more details are available online at <http://pmip3.lsce.ipsl.fr/>. The observational data used for model evaluation are obtained from the European Center for Medium Range Weather Forecast ERA-interim reanalysis data (Dee *et al.*, 2011). Both model and observational data were first bilinearly interpolated to a horizontal resolution of $2.0^\circ \times 2.0^\circ$ for further comparison, which is the mid-range level for models.

Model performance was assessed by comparing the spatial distributions between simulations and observations for the period 1979–2005. As the primary features of the EAM are southerly winds loading warm and moist air masses from the South China Sea and Bay of Bengal in summer and strong northerly winds from the cold-core Siberia–Mongolia in winter (Ding, 1994), low-level meridional wind fields were applied for evaluation. Here, we referred to the method used by Jiang and Tian (2013). Specifically, summer (June, July and August) evaluation was performed on the 850 hPa meridional wind over 63 grid points within the region of 20° – 40° N and 105° – 120° E, and as three models did not release wind data at 10 m, winter (December, next January and February) evaluation was performed on meridional wind at two levels of 10 m and 925 hPa within the regions of 25° – 40° N and 120° – 140° E together with 10° – 25° N and 110° – 130° E on 123 grid points. To objectively measure the ability of models to simulate the EAM, spatial correlation coefficients (SCC) and normalized centred root mean square differences (RMSD)

TABLE 1 Details of the model simulations used in this study

| Model ID | Model name | Country | Atmospheric resolution | Time span | No data for wind at 10 m |
|----------|----------------|-----------|------------------------|-----------|--------------------------|
| 1* | CCSM4 | USA | 1.25° × ~0.9°, L26 | 850–1850 | √ |
| 2* | CSIRO-Mk3L-1-2 | Australia | ~5.6° × ~3.2°, L18 | 851–1850 | √ |
| 3 | FGOALS-gl | China | 5.0° × ~4.0°, L26 | 1000–1999 | √ |
| 4* | FGOALS-s2 | China | ~2.8° × ~1.7°, L26 | 850–1850 | |
| 5* | GISS-E2-R | USA | 2.5° × 2.0°, L40 | 850–1850 | |
| 6* | HadCM3 | UK | 3.75° × 2.5°, L19 | 850–1850 | |
| 7* | IPSL-CM5A-LR | France | 3.75° × ~1.9°, L39 | 850–1850 | |
| 8* | MPI-ESM-P | Germany | ~1.9° × ~1.9°, L47 | 850–1849 | |
| 9* | MRI-CGCM3 | Japan | ~1.1° × ~1.1°, L48 | 850–1850 | |

Note: Model IDs with asterisks represent those with historical runs for assessment covering from 1979 to 2005.

of each simulation with respect to observations were calculated model by model. Model selection was based on the criterion that the SCC is statistically significant at the 99% confidence level together with the normalized centered RMSD being less than 1.00. On this basis, the median value of the chosen models was adopted to represent the overall estimate.

Although the timing and spatial structure of the MCA and LIA are complex, with different reconstructions exhibiting warm and cold conditions at different times for different regions and seasons, the Northern Hemisphere temperature reconstructions indicated mostly warmer conditions from about 950 to about 1250 and colder conditions from about 1450 to about 1850 (PAGES 2k Consortium, 2013). For the convenience of calculation, we considered these two intervals the MCA and LIA, respectively.

3 | RESULTS

There are several approaches to quantify the intensities of the EASM and EAWM, which are measured from perspectives involving sea-level pressure (SLP) gradient, meridional and/or zonal winds in the lower or upper troposphere and geopotential height in the middle troposphere (Wang *et al.*, 2008; Wang and Chen, 2010). Considering that the monsoon originates from the land–sea thermal contrast and is intrinsically related to the low-level air temperature, SLP and wind fields, we used two indices measured by the wind and SLP gradient, respectively, to quantitatively depict the EAM intensity. One index used the regionally averaged summer meridional wind at 850 hPa within the region of 20°–40°N and 105°–120°E to quantify the EASM, and the winter meridional wind at 10 m was averaged within the regions of 25°–40°N and 120°–140°E together with 10°–25°N and 110°–130°E to quantify the EAWM.

The percentage change in these values relative to their 850–1850 climatology for each model was regarded as the EASM or EAWM intensity index, hereafter referred to as the meridional wind (MW)-index. The other index is defined as the zonal SLP difference between a land longitude over East Asia and an oceanic longitude over the western North Pacific (Guo, 1994; Guo *et al.*, 2003), namely, the SLP-index.

3.1 | Evaluation of the PMIP3 models and change in the EASM

Figure 1a displays the SCCs and normalized centred RMSDs between the simulated and observed climatology of the meridional wind at 850 hPa in summer. It shows that seven of the eight models have statistically significant SCCs at the 99% confidence level ranging from 0.51 to 0.72, except for CSIRO-Mk3L-1-2, which shows a negative correlation. The normalized centred RMSDs range from 0.74 to 1.35, with the values of CSIRO-Mk3L-1-2 and FGOALS-s2 larger than 1.00. Given that not all the models meet the requirement we defined and that FGOALS-gl is not available for model assessment, we eliminated this model in order to avoid the potential uncertainties it may bring. Thus, six models were chosen for the following analysis.

As shown in Figure 2, the EASM intensity varies slightly over the whole past millennium with all the models exhibiting decreasing trends either for the MW-index or SLP-index. However, statistically significantly decreased trends at the 95% confidence level are identified in only two models (GISS-E2-R and IPSL-CM5A-LR) and the six-model median estimate in the MW-index and in four models (CCSM4, GISS-E2-R, HadCM3 and MRI-CGCM3) and the six-model median estimate in the SLP-index.

In the case of the MCA, the EASM change was simulated at a high-level model consistency, with five of the

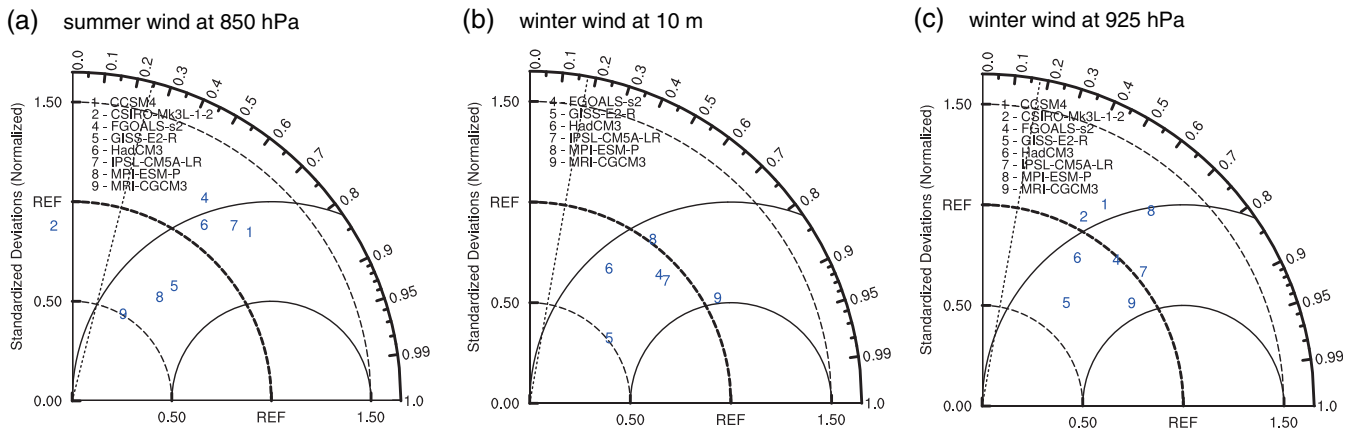
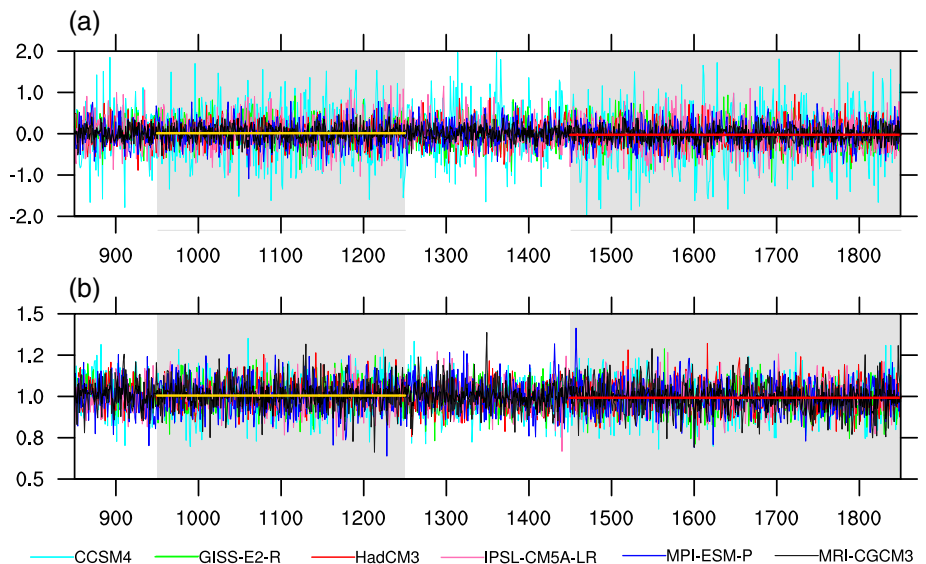


FIGURE 1 Taylor diagrams (Taylor, 2001) displaying the normalized pattern statistics of climatological meridional wind (a) at 850 hPa within the region of 20°–40°N and 105°–120°E between the eight climate models and observations in summer and (b) at 10 m and (c) 925 hPa within the regions of 25°–40°N and 120°–140°E together with 10°–25°N and 110°–130°E between the six and eight climate models, respectively, and observations in winter for the reference period of 1979–2005. Each number represents a model ID (see Table 1), and the observation is considered the reference (REF). Standard deviation and centred root mean square difference are normalized by the REF standard deviation. The radial distance from the origin is the normalized standard deviation of a model; the correlation between a model and the REF is given by the azimuthal position of the model, with the oblique dotted line showing the 99% confidence level, and the normalized centred root mean square difference between a model and the REF is their distance apart. Briefly, the nearer the distance between a number and REF, the better the performance of the corresponding model [Colour figure can be viewed at wileyonlinelibrary.com]

FIGURE 2 East Asian summer monsoon intensity indices as measured by (a) meridional wind at 850 hPa and (b) zonal sea-level pressure difference, in which black curves represent the six-model median estimates, and yellow and red lines denote the mean values averaged over the MCA and LIA based on median estimates, respectively. Grey dashed areas indicate the MCA and LIA periods. MCA, Medieval Climate Anomaly; LIA, Little Ice Age [Colour figure can be viewed at wileyonlinelibrary.com]



six models showing strengthening during the MCA (Figure 3a,c). At the regional scale, the models showed warming over and around the East Asian region (Figure 4a). However, owing to the different heat contents between the land and ocean, the temperature over the Asian continent increased with a larger magnitude than over the neighbouring oceans, which generated an anomalous Asian continental low at the lower level. Thereafter, on the one hand, meridional SLP gradient increased over East Asia and the South China Sea, leading to the development of the cross-equatorial current off the Somali coast and deepening and northward migration of the monsoon trough over the Bay

of Bengal. This accelerated the eastward propagation of low-level moist westerlies across India and resulted in enhanced Indian monsoonal precipitation in the Indian Peninsula. On the other hand, the reinforced thermal contrast between East Asia and the same latitudes of the western North Pacific led to an intensified zonal SLP gradient and, in turn, generated southerly wind anomalies over East Asia. Therefore, more warm water vapour from the South China Sea and the western North Pacific moved towards south-eastern China and the Yangtze River Basin and then generated increased precipitation. In addition, an anomalous positive SLP centre was

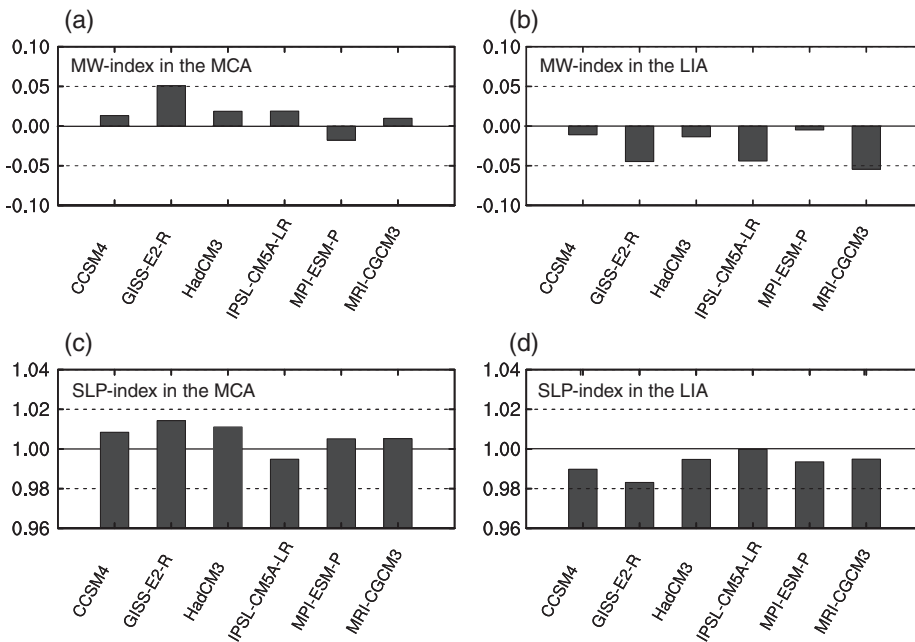


FIGURE 3 East Asian summer monsoon intensity indices in the Medieval Climate Anomaly (left) and Little Ice Age (right) for individual models. Top and bottom panels show the meridional wind-index and sea-level pressure-index, respectively

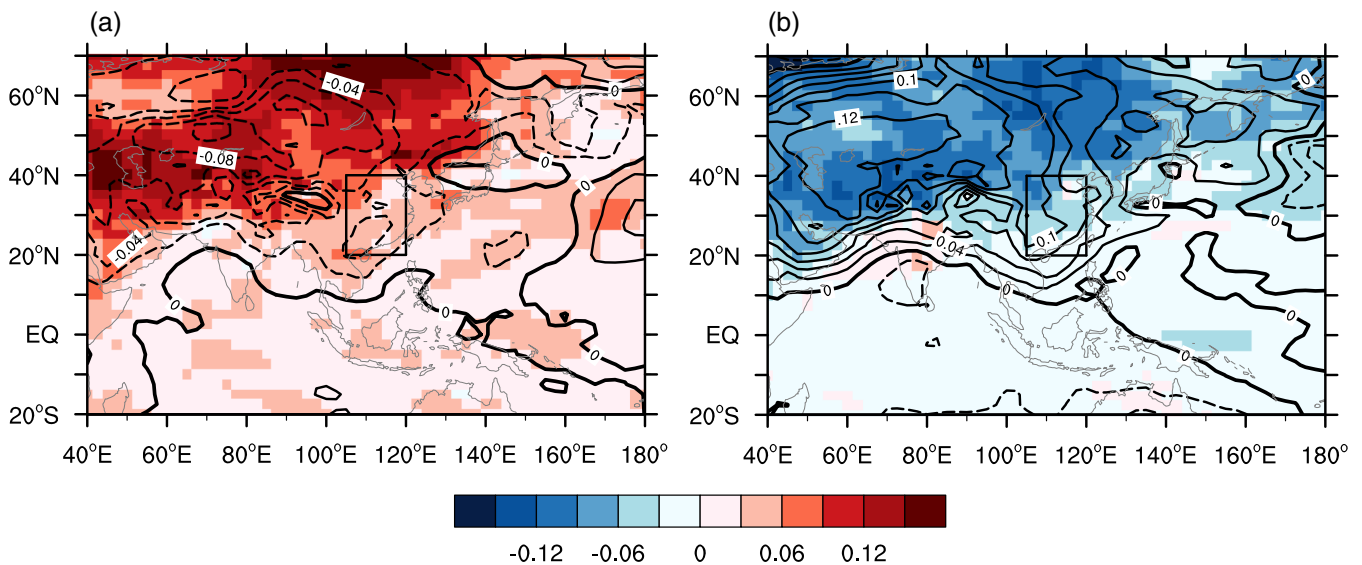


FIGURE 4 Changes in summer temperature (shading; units: K) and sea-level pressure (contour; units: hPa) in the (a) Medieval Climate Anomaly and (b) Little Ice Age with reference to the period of 850–1850 as derived from the six-model median estimate. The rectangle indicates the region of 20°–40°N and 105°–120°E [Colour figure can be viewed at wileyonlinelibrary.com]

established over the Japan Sea due to the warming contrast, hence guiding south-easterly anomalies at its southern edge to transport moisture from the Pacific to the Yellow River Basin and bring more precipitation to that region (Figure 5b). For the upper troposphere, the 200 hPa subtropical westerly jet stream, which is another major component of the EASM system, indicated a weakened feature (Figure 6b). It was the aforementioned meridional warming difference between the land and ocean that weakened the temperature gradient from higher to lower latitudes on a hemispheric scale, which reduced the baroclinic feature that

extended to the upper troposphere. Consequently, heating-induced mass change lowered the meridional temperature contrast and then weakened the subtropical westerly jet. The decreased EASM was also identified at the middle level, where a strengthened western Pacific subtropical high was found extending straight upward to the middle troposphere, and its centre barely moved (Figure 7b).

In the context of the LIA, the EASM behaved in the opposite way, with all the six models showing decreased strength (Figure 3b,d). Specifically, the temperature over the Asian continent cooled more than the surrounding

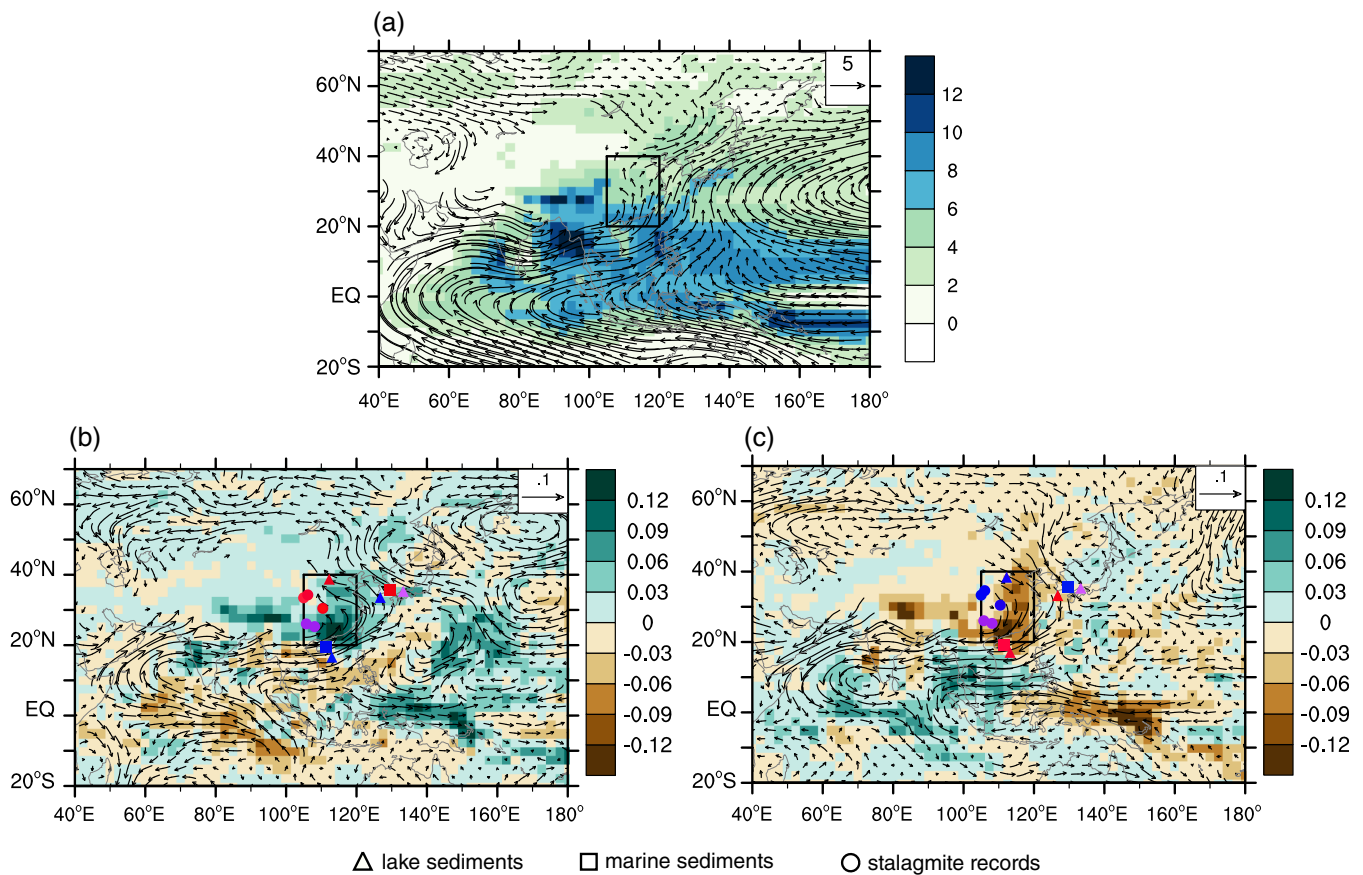


FIGURE 5 (a) Climatology of summer wind (vector; units: $\text{m}\cdot\text{s}^{-1}$) at 850 hPa and precipitation (shaded; units: $\text{mm}\cdot\text{day}^{-1}$) for 850–1850 from the six-model median estimates and the corresponding differences in the (b) Medieval Climate Anomaly and (c) Little Ice Age with reference to 850–1850. The rectangles are the same as in Figure 4. The locations of Dongge Cave (Wang *et al.*, 2005), Heshang Cave (Hu *et al.*, 2008), Wanxiang Cave (Zhang *et al.*, 2008), Huangye Cave (Tan *et al.*, 2010), Dongdao Island (Yan *et al.*, 2011), Gonghai Lake (Chen *et al.*, 2015), core TY08PC1 (Lee and Park, 2015), Yelang Cave (Zhao *et al.*, 2015), Qionghai (Deng *et al.*, 2017), Mulyoungari Swamp (Park *et al.*, 2017) and Nakaumi Lake (Yamada *et al.*, 2019) are marked, with red, blue and purple representing strong, weak and no obvious changes in EASM during the corresponding periods, respectively [Colour figure can be viewed at wileyonlinelibrary.com]

oceans, causing a rising SLP across the continent (Figure 4b). This implies a reduced meridionally SLP gradient in southern East Asia and a suppressed zonal SLP gradient in eastern East Asia. Therefore, on the southern coastal Asian continent, an anomalous easterly wind weakened the monsoon trough and reduced the moisture transport from the Arabian Sea to the India Peninsula and from the Bay of Bengal and South China Sea to East Asia; thus, less precipitation was simulated in both India and southeastern China (Figure 5c). In addition, on the eastern coast of Asia, in the presence of a negative SLP centre over the northern Pacific, anomalous northerly and northwesterly winds formed, which lowered the vapour transportation from the subtropical western Pacific to the Asian continent, leading to deficient precipitation in central and northeastern China. In contrast to the MCA, the high-level subtropical westerly jet stream intensified due to the strengthened low-level meridional temperature contrast, and the mid-level western Pacific

subtropical high showed a weakened feature (Figures 6c and 7c).

Changes in the EASM intensity during these two periods are also confirmed by previous single-model simulations (Peng *et al.*, 2010; Liu *et al.*, 2011; Man *et al.*, 2012; Landrum *et al.*, 2013; Man and Zhou, 2014). These model simulations showed better agreement in terms of changes in atmospheric circulation than that of precipitation, which is in accordance with the PMIP3 results. Overall, the majority of the models demonstrated a synchronous in-phase precipitation change over the whole monsoonal region, but CCSM4 from the PMIP3 and FGOALS-g1 (Man and Zhou, 2014) presented a meridional tripole pattern change in both the MCA and LIA over East Asia, and HadCM3 from the PMIP3 showed a meridional tripole pattern only during the LIA. It is widely accepted that ENSO plays a role in influencing the EASM; the inconsistent precipitation pattern might be generated from the different sea surface temperature

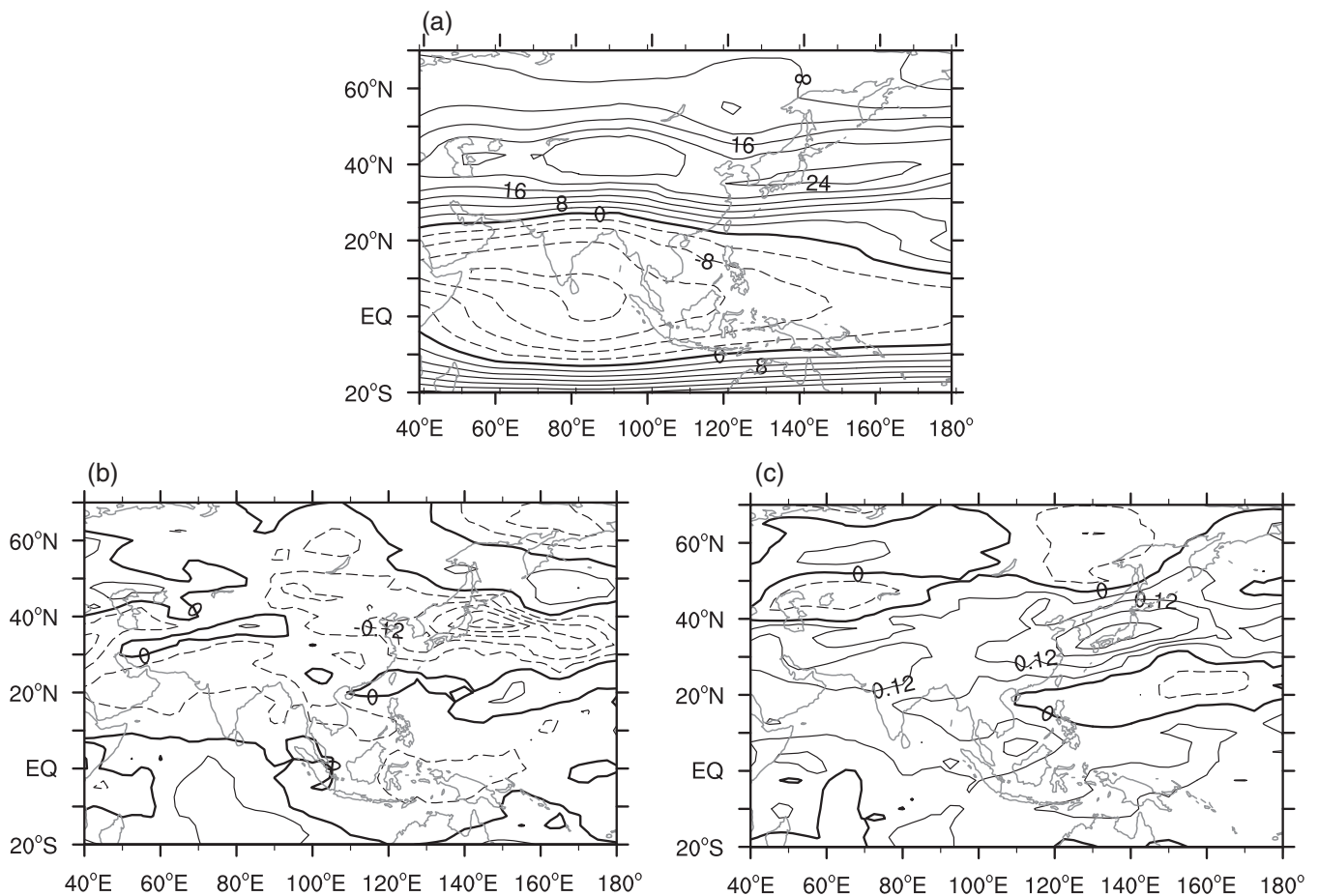


FIGURE 6 (a) Climatology of zonal wind (units: $\text{m}\cdot\text{s}^{-1}$) at 200 hPa for 850–1850 from the six-model median estimates and the corresponding difference in the (b) Medieval Climate Anomaly and (c) Little Ice Age with reference to 850–1850

patterns and also ENSO-related physical processes, for example, the Indo-western Pacific ocean capacitor (Xie *et al.*, 2016), simulated from model to model.

The EASM intensity during the last millennium has been reconstructed from multiple types of geological archives, including stalagmite records (Wang *et al.*, 2005; Hu *et al.*, 2008; Zhang *et al.*, 2008; Tan *et al.*, 2010; Zhao *et al.*, 2015), fossil pollen and ostracods from lake sediments (Yan *et al.*, 2011; Chen *et al.*, 2015; Li *et al.*, 2017; Yamada *et al.*, 2019) and marine sediments (Lee and Park, 2015; Deng *et al.*, 2017). Most of these reconstructions are indicators of precipitation variation, and they demonstrated a degree of regional feature (Figure 5b,c). Generally, proxy sites located in the northern monsoonal region showed a stronger EASM during the MCA than during the LIA (Hu *et al.*, 2008; Zhang *et al.*, 2008; Tan *et al.*, 2010; Chen *et al.*, 2015; Li *et al.*, 2017), which is consistent with the finding of multiple simulations, whereas those located in the southeastern region exhibited insignificant EASM differences between the two periods but centennial scale variations (Zhao *et al.*, 2015) or an increasing trend beginning in the late MCA (Wang *et al.*, 2005). Moreover,

two lake sediments (Park *et al.*, 2017; Yamada *et al.*, 2019) and one marine sediment (Lee and Park, 2015) showed conflicting changes around South Korea and southwest Japan. Park *et al.* (2017) further noted that this may be because rainfall in coastal East Asia is extraordinarily complex as it is influenced not only by EASM but also by ENSO-modulated typhoons.

Recently, some studies have noted that $\delta^{18}\text{O}$ signals recorded in stalagmites reflect changes in moisture sources or water vapour pathways rather than precipitation changes (LeGrande and Schmidt, 2009; Dayem *et al.*, 2010; Liu *et al.*, 2015). Therefore, the centennial scale difference between the northern and southern located stalagmite data may be due to the water vapour in the southwestern monsoonal region being mostly from the Bay of Bengal than from the western Pacific, while that of the northeastern part is the opposite.

In summary, model simulations and geological evidence coincide well with each other and suggest a strengthened EASM in the MCA and the opposite in the LIA. Uncertainties exist in both models and reconstructions. This is because, on the one hand, the capability of models in

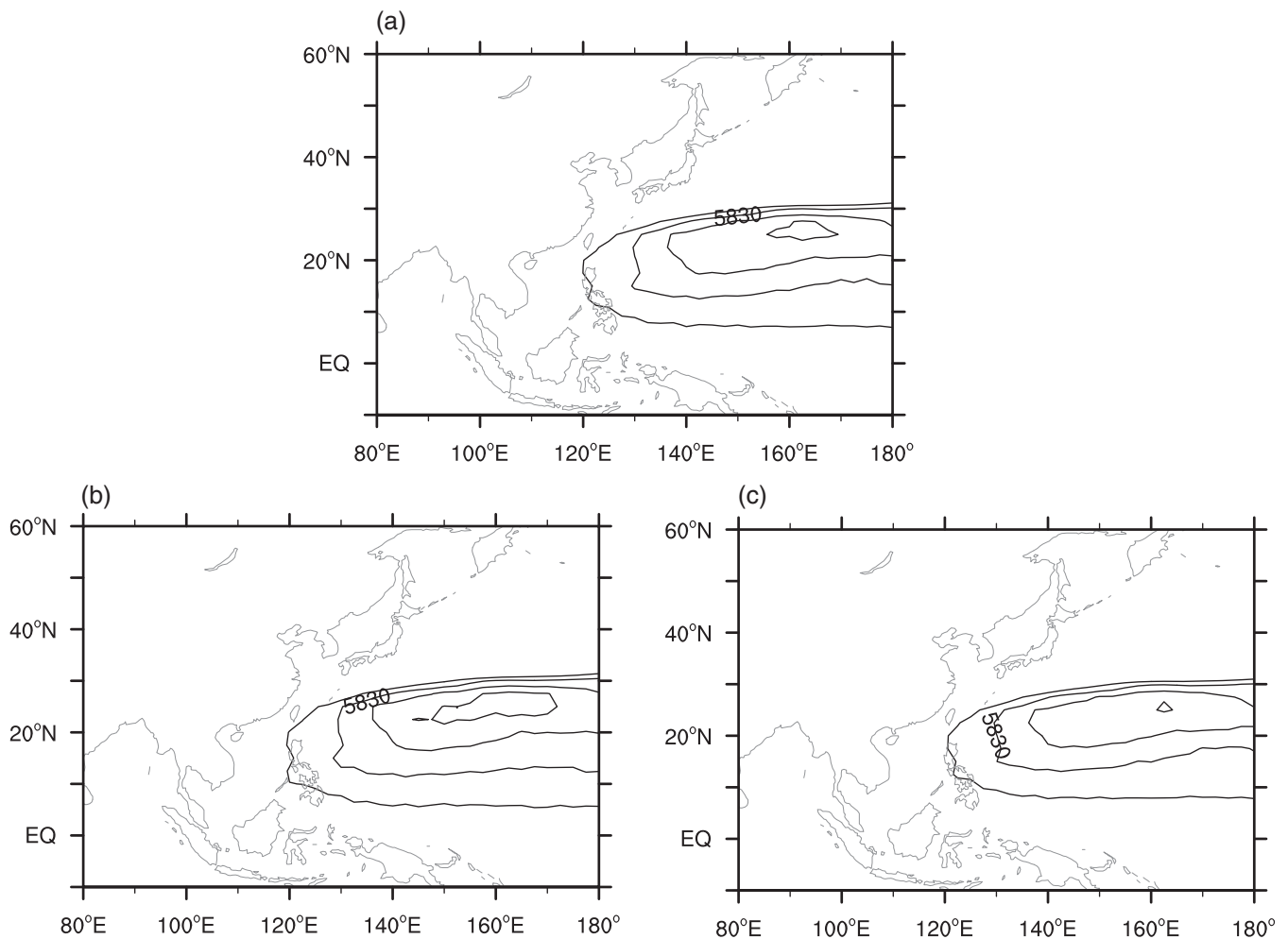


FIGURE 7 Same as Figure 6 but for the West Pacific subtropical high from the 500 hPa geopotential height (units: gpm)

accurately depicting the monsoon system is still inadequate, and on the other hand, diverse proxy types and reconstruction methods generated discrepancies across different monsoonal regions and among different EASM reconstructions. In addition, information interpreted from most of these proxies is annual climatic signals, leading to an insufficient ability in distinguishing summer signals from other seasonal signals.

3.2 | Evaluation of the PMIP3 models and change in the EAWM

In Figure 1b,c, winter meridional wind assessments show that the SCCs are all statistically significant at the 99% confidence level with values from 0.51 to 0.87 and from 0.47 to 0.82, and the corresponding normalized centred RMSDs are from 0.52 to 0.90 and from 0.57 to 1.07 at levels of 10 m and 925 hPa, respectively. Besides, those who have both levels of wind data showed similar performances at the two levels. Considering that the normalized centred RMSDs of CCSM4

and CSIRO-Mk3L-1-2 are greater than 1.00 in the 925 hPa assessment, and that both of these two models did not release 10 m wind data, we eliminated these two models and utilized 10 m wind data of the remaining six models for the following investigation.

Figures 8 and 9 show that the EAWM indices present little long-term trend throughout the millennium. In detail, FGOALS-s2 and HadCM3 demonstrated increased trends, whereas GISS-E2-R, IPSL-CM5A-LR, MPI-ESM-P and MRI-CGCM3 presented decreased trends in both the MW-index and SLP-index. However, only increased trend of FGOALS-s2 and decreased trend of MRI-CGCM3 for the MW-index are statistically significant at the 95% confidence level, and no statistically significant trend was detected for the SLP-index. Overall, changes in the EAWM intensity are dependent on model and index.

The EAWM mostly dominates the northerly wind along coastal East Asia and is driven by SLP differences between the Siberian High and Aleutian Low. As shown in Figure 11a, the winter monsoonal circulation during

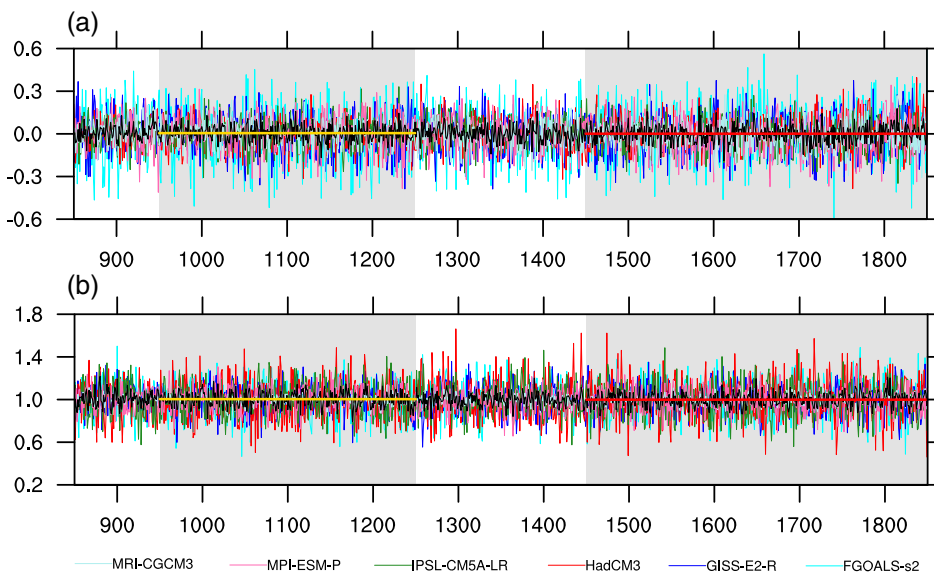


FIGURE 8 East Asian winter monsoon intensity indices as measured by the (a) meridional wind at 10 m and (b) zonal sea-level pressure difference, in which the black curves represent the six-model median estimates, and the yellow and red lines show their mean values averaged over the MCA and LIA, respectively. Grey dashed areas indicate the MCA and LIA periods. MCA, Medieval Climate Anomaly; LIA, Little Ice Age [Colour figure can be viewed at wileyonlinelibrary.com]

the last millennium has a pattern that is similar to the modern EAWM (Chen *et al.*, 2000). It can be separated into two components; the northern component is in the region north of 25°N , where northwesterly winds are separated into two branches: one that moved east through southern Japan to the subtropical western and central Pacific and the other that flowed along the coastline of East Asia. The southern component is in the region south of 25°N , where the northeasterly flow mainly prevailed.

With respect to the MCA, the majority of models simulated increased temperature changes in most of the Northern Hemisphere, with higher latitudes experiencing more heating (Figure 10a). However, because of the large spread among models in characterizing the distribution of positive and negative temperature centres from Siberia to the Aleutian Islands, four (two) of the six models exhibited an intensified (weakened) Siberian High, and five (one) reproduced a weakened (strengthened) Aleutian Low. Therefore, in the northern part of the EAWM region, an enhanced Aleutian Low led to strengthened meridional SLP contrast between the Aleutian Islands and North Pacific and consequently generated an anomalous westerly flow over the Yellow Sea and southern Japan, indicating an intensified EAWM (Figure 11b). However, the simulations in the southern part of the EAWM region are highly debated. Three models showed a warmer continent than the same latitudes of the ocean, while the other three models exhibited reversed thermal changes or a similar degree of warming. Therefore, the northerly flow shown in the median estimate is largely uncertain (Figure 11b). In the middle troposphere, a stronger East Asian trough at 500 hPa geopotential height was detected in most models during this period, which confirms a strengthened EAWM.

With regard to the LIA, most models simulated southerly anomalies along coastal East Asia (Figure 11c), indicating a weakened EAWM. In detail, temperature presented the largest decrease over the Aleutian Islands compared with Siberia and the mid-latitude North Pacific in four of the six models. Consequently, the SLP ascended over the Aleutian Islands and was slightly suppressed over the Siberian region, resulting in a weakened and northward shifted Aleutian Low and a suppressed Siberian High (Figure 10b), consequently generating southerly winds over the northern component of the EAWM key region (Figure 11c). In addition, the East Asian trough at 500 hPa geopotential height was consistently weakened. However, situations in the southern part are similar to those in the MCA, with models showing diverse changes in temperature, SLP difference and winds.

Modern climatological studies considered EAWM to be an essential link between mid-latitude and tropical circulations, and its impact on the South China Sea and eastern Pacific was illustrated as a predicting tool for the following summer monsoon (Chen *et al.*, 2000; Wang and Chen, 2010). On the interannual-to-interdecadal scale, variability of the EAWM system was distinguished as two unique northern and southern modes. The northern mode is preceded by excessive autumn snow cover in southern Siberia–Mongolia, whereas the southern mode is related to the ENSO (Wang *et al.*, 2010; Chen *et al.*, 2014). During winter, ENSO largely modulated East Asian water vapour transport through the access of the Pacific–East Asian teleconnection (Wang *et al.*, 2000), and the central and eastern tropical Pacific sea surface temperature-associated teleconnection was also lately identified as a crucial factor impacting the water vapour transport over East Asia (Sun *et al.*, 2019). This explains,

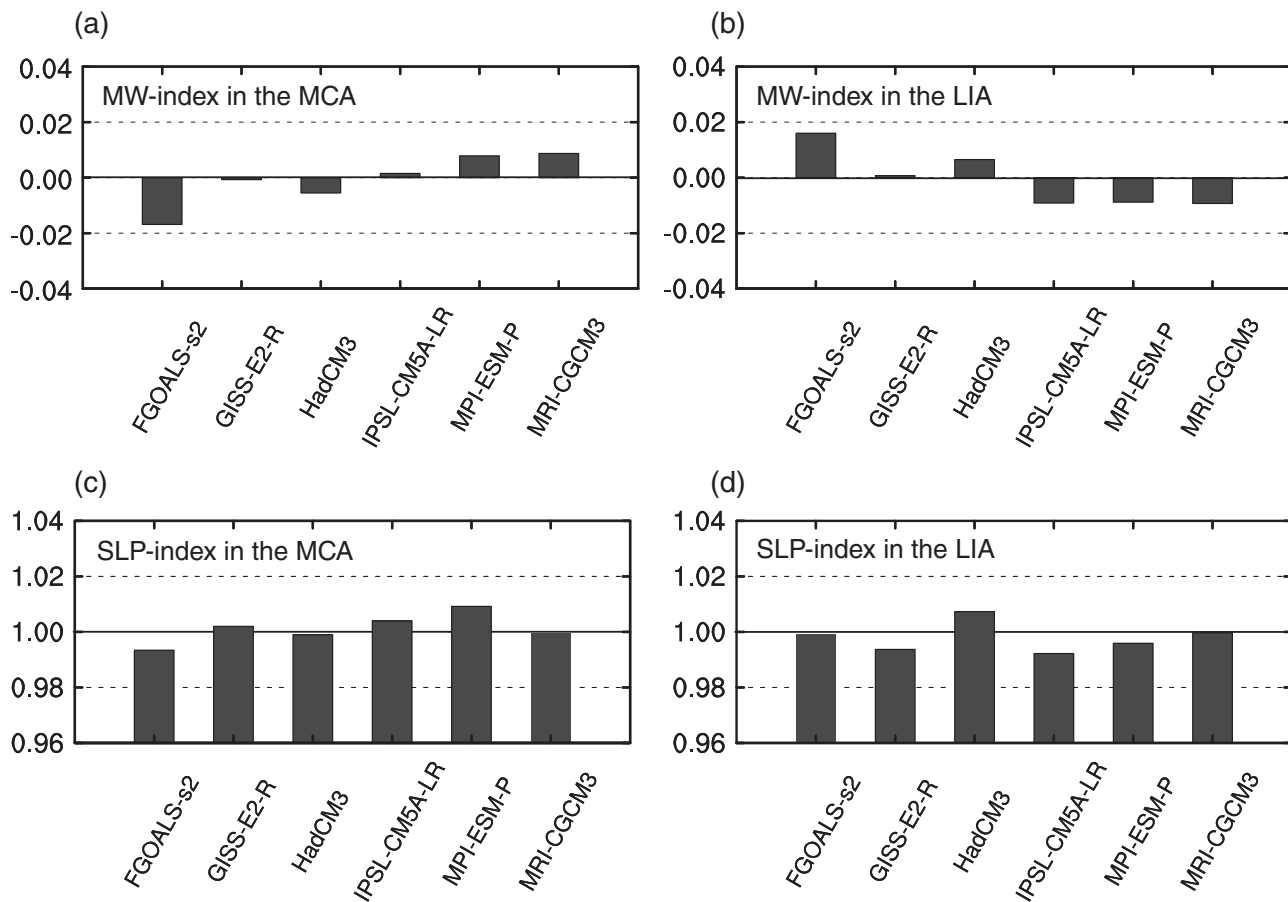


FIGURE 9 Same as Figure 3 but for East Asian winter monsoon intensity indices

to a certain extent, the performance of multiple models showing some skills in simulating the northern component of the EAWM but exhibiting diverse results for the southern component when involved in complex extratropical–tropical and air–sea interactions. It is also worth noting that enhanced precipitation was simulated over Indonesia and that the opposite was found over the Philippines and mid-latitude western Pacific (Figure 11b). This agrees with previous findings showing that a strong EAWM facilitates excessive precipitation in low latitudes and deficient precipitation over mid-latitudes based on modern observations (Wang and Chen, 2010).

Grain size of sediments, foraminiferal $\delta^{18}\text{O}$ data and diatom assemblages from marine sediments and elemental ratios in Chinese loess deposits are commonly used proxies for reconstructing the Holocene EAWM evolution (Wang *et al.*, 2012; Liu *et al.*, 2013; Li and Morrill, 2014; Sagawa *et al.*, 2014; Li *et al.*, 2018). However, these pieces of geological evidence mostly have low temporal resolutions and show conflicting results during the past millennium (Figure 11b,c). For example, in northwestern East Asia, reconstructions derived from aeolian sediments (Liu *et al.*, 2013) and lake deposits (Liu *et al.*, 2009)

showed a stronger EAWM in the MCA than in the LIA, which is in accordance with the model simulations in this study. However, between these two sites, aeolian sediments (Li and Morrill, 2014) and a peat record (Yu *et al.*, 2011) indicated multiple time scale variations rather than a centennial scale difference. For southeastern East Asia, a stronger (weaker) northerly wind was interpreted by the total organic carbon contents and titanium concentrations (Yancheva *et al.*, 2007), as well as by diatom assemblages (Wang *et al.*, 2012) from Huguang Maar Lake, indicating a reinforced (weakened) EAWM during the MCA (LIA). However, for the western North Pacific, conflicting results are found in the marine sediments from northern Japan (Sagawa *et al.*, 2014) and the southern Okinawa Trough (Li *et al.*, 2018). In addition, based on nine mean grain size records of muddy sediments from Chinese coastal seas dating back to 3,000 years ago, Tu *et al.* (2017) found large discrepancies in EAWM intensity among different records. The researchers further noted that those located far from the river estuary mostly showed weak EAWM strength during the MCA and enhanced strength during the LIA.

In a word, multiple model simulations show that the EAWM is slightly stronger during the MCA than that

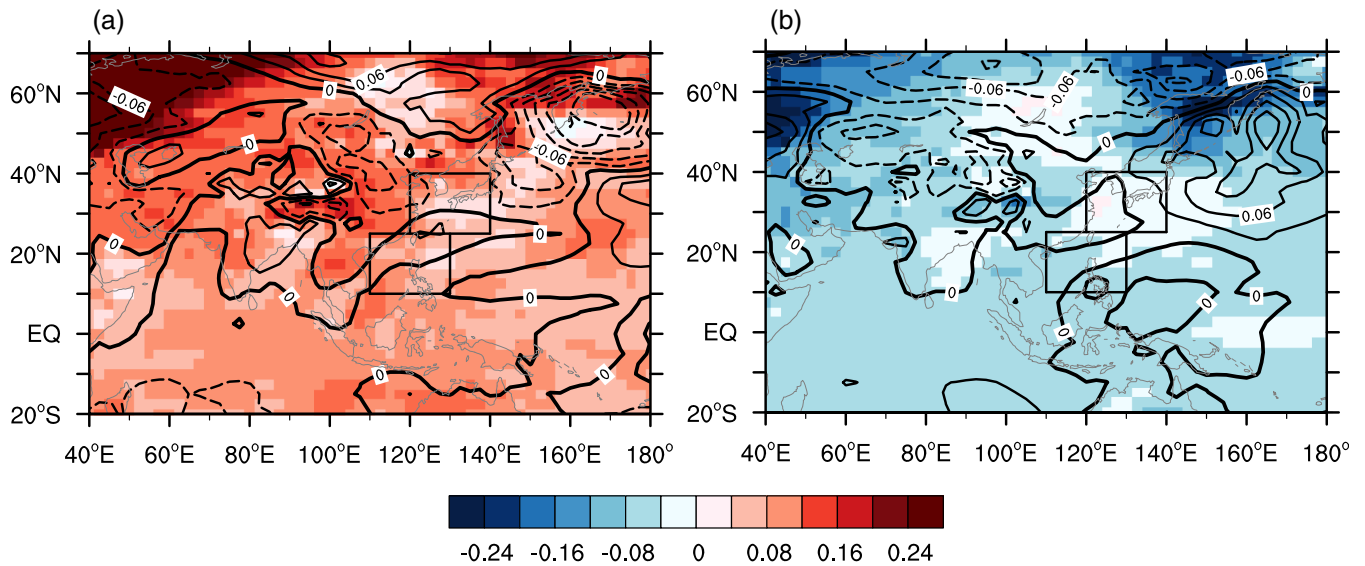


FIGURE 10 Changes in winter temperature (shading; units: K) and sea-level pressure (contour; units: hPa) in the (a) Medieval Climate Anomaly and (b) Little Ice Age with reference to the period of 850–1850 as derived from the six-model median estimate. The rectangles show the regions of 10°–25°N and 110°–130°E, and 25°–40°N and 120°–140°E [Colour figure can be viewed at wileyonlinelibrary.com]

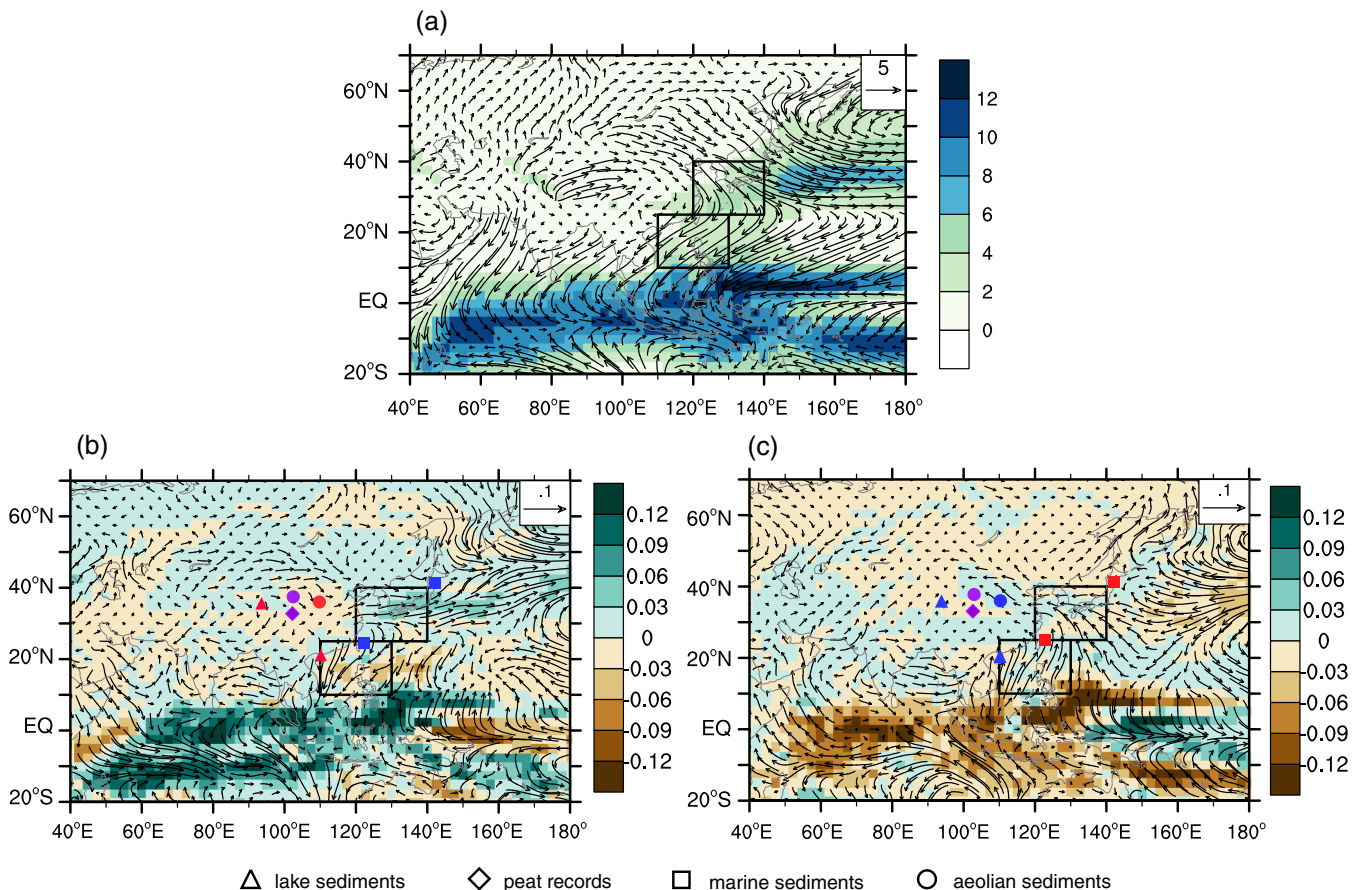


FIGURE 11 (a) Climatology of winter wind (vector; units: $\text{m}\cdot\text{s}^{-1}$) at 10 m and precipitation (shaded; units: $\text{mm}\cdot\text{day}^{-1}$) for 850–1850 as derived from the six-model median estimates and the corresponding differences in the (b) Medieval Climate Anomaly and (c) Little Ice Age with reference to 850–1850. The rectangles are the same as in Figure 10. The locations of Huguang Maar Lake (Yancheva *et al.*, 2007; Wang *et al.*, 2012), Kusai Lake (Liu *et al.*, 2009), Hongyuan Swamp (Yu *et al.*, 2011), Gonghe Basin (Liu *et al.*, 2013), Huangyanghe (Li and Morrill, 2014), core SK-2 (Sagawa *et al.*, 2014) and core MD05-2908 (Li *et al.*, 2018) are marked, with red, blue and purple representing strong, weak and no obvious changes in East Asian winter monsoon during the corresponding periods, respectively [Colour figure can be viewed at wileyonlinelibrary.com]

during the LIA for the northern component of the EAWM, and the changes during both periods at the southern component are controversial. Uncertainties come from the different model responses to external forcings, as well as diverse modelling skills in simulating air–sea and extratropical–tropical interactions. Moreover, spatial and temporal discrepancies are evident in the EAWM reconstructions during the last millennium. This is due to sparse suitable archives and proxies (Sagawa *et al.*, 2014); age uncertainties; and other influencing factors such as sedimentary environments, riverine runoff and storms (Tu *et al.*, 2017). All the above makes the conclusion less trustworthy. Therefore, reconstructions in higher temporal and spatial resolutions, together with sources of reliable types of proxy and methods, are needed to precisely characterize the EAWM intensity in order to test model simulations and better understand the mechanisms of the EAWM during the past millennium.

4 | CONCLUSIONS

Based on nine simulations of the last millennium from the PMIP3, the EASM and EAWM changes and their underlying mechanisms in the warm MCA and cold LIA were assessed in this study. The main results are as follows:

The EASM during the MCA is stronger than that during the LIA, and most of the reconstructions support this result, although discrepancies exist among different records. The monsoonal region shows anomalous southerly winds in the lower level, a strengthened western Pacific subtropical high in the middle level and an intensified subtropical westerly jet stream in the higher level, together with excessive precipitation over East Asia during the MCA and inverted situations in the LIA. The main factor responsible for the changes in the EASM system is the land–sea thermal contrast.

The variations in EAWM indices are dependent on model and index. The EAWM system shows different changes between the low latitudes and the mid-to-high latitudes during the MCA and LIA periods. In the northern part of the EAWM region, a high-latitude temperature change is the main driver of the associated circulation. It generates a strengthened Aleutian Low that guides the westerly wind anomalies at its southern edge during the MCA, whereas a weakened and northward shifted Aleutian Low, as well as a slightly strengthened Siberian High, result in a southerly flow in the LIA, indicating an intensified EAWM in the MCA and a weakened EAWM in the LIA. However, for the southern part of the EAWM region, controversial results were simulated among individual models, leading to large uncertainty.

Collectively, climate models show a better ability to reproduce the EAM system when underlying thermal changes act as the dominant driving factor, and more efforts should be made to improve the model skill in demonstrating regional scale processes and internal climate interactions, especially for the EAWM.

ACKNOWLEDGMENTS

We acknowledge all the climate modelling groups in the PMIP project (listed in Table 1) for producing and sharing their model output. This research was jointly supported by the National Natural Science Foundation of China (grant 41775072), the National Key R&D Program of China (grant 2018YFC1505702), the Outstanding Young Talents Project of Sichuan Province (grant 2019JDJQ0001) and the Scientific Research Foundation of Key Laboratory of Meteorological Disaster, Ministry of Education (grant KLME201803).

ORCID

Kaiqing Yang  <https://orcid.org/0000-0002-3902-5024>

Wei Hua  <https://orcid.org/0000-0003-2496-3592>

Qin Hu  <https://orcid.org/0000-0002-8576-299X>

REFERENCES

- Anchukaitis, K.J., Buckley, B.M., Cook, E.R., Cook, B.I., D'Arrigo, R.D. and Ammann, C.M. (2010) Influence of volcanic eruptions on the climate of the Asian monsoon region. *Geophysical Research Letters*, 37, L22703.
- Chen, F., Xu, Q., Chen, J., Birks, H.J.B., Liu, J., Zhang, S., Jin, L., An, C., Telford, R.J., Cao, X., Wang, Z., Zhang, X., Selvaraj, K., Lu, H., Li, Y., Zheng, Z., Wang, H., Zhou, A., Dong, G., Zhang, J., Huang, X., Bloemendal, J. and Rao, Z. (2015) East Asian summer monsoon precipitation variability since the last deglaciation. *Scientific Reports*, 5, 11186.
- Chen, W., Graf, H.-F. and Huang, R. (2000) The interannual variability of east Asian winter monsoon and its relation to summer monsoon. *Advances in Atmospheric Sciences*, 17, 48–60.
- Chen, Z., Wu, R. and Chen, W. (2014) Distinguishing interannual variations of the northern and southern modes of the east Asian winter monsoon. *Journal of Climate*, 27, 835–851.
- Dayem, K.E., Molnar, P., Battisti, D.S. and Roe, G.H. (2010) Lessons learned from oxygen isotopes in modern precipitation applied to interpretation of speleothem records of paleoclimate from eastern Asia. *Earth and Planetary Science Letters*, 295, 219–230.
- Dee, D.P., Uppala, S.M., Simmons, A.J., Berrisford, P., Poli, P., Kobayashi, S., Andrae, U., Balmaseda, M.A., Balsamo, G., Bauer, P., Bechtold, P., Beljaars, A., van de Berg, L., Bidlot, J., Bormann, N., Delsol, C., Dragani, R., Fuentes, M., Geer, A.J., Haimberger, L., Healy, S.B., Hersbach, H., Hólm, E.V., Isaksen, I., Kallberg, P., Köhler, M., Matricardi, M., McNally, A. P., Monge-Sanz, B.M., Morcrette, J.-J., Park, B.K., Peubey, C., de Rosnay, P., Tavolato, C., Thépaut, J.-N. and Vitart, F. (2011) The ERA-interim reanalysis: Configuration and performance of

- the data assimilation system. *Quarterly Journal of the Royal Meteorological Society*, 137, 553–597.
- Deng, W., Liu, X., Chen, X., Wei, G., Zeng, T., Xie, L. and Zhao, J.-X. (2017) A comparison of the climates of the medieval climate anomaly, little ice age, and current warm period reconstructed using coral records from the northern South China Sea. *Journal of Geophysical Research: Oceans*, 122, 264–275.
- Ding, Y. (1994) *Monsoons over China*. Dordrecht, The Netherlands: Kluwer Academic Publisher, p. 419.
- Ding, Y., Wang, Z. and Sun, Y. (2008) Inter-decadal variation of the summer precipitation in East China and its association with decreasing Asian summer monsoon. Part I: Observed evidences. *International Journal of Climatology*, 28, 1139–1161.
- Fang, K., Davi, N. and D'Arrigo, R. (2014) A reconstruction of the Asia-Pacific oscillation index for the past 1500 years and its association with the Asian summer monsoon. *International Journal of Climatology*, 34, 2505–2514.
- Guo, Q.Y. (1994) Relationship between the variations of east Asian winter monsoon and temperature anomalies in China (in Chinese). *Quarterly Journal of Applied Meteorology*, 5, 218–225.
- Guo, Q.Y., Cai, J.N., Shao, X.M. and Sha, W.Y. (2003) Interdecadal variability of east-Asian summer monsoon and its impact on the climate of China (in Chinese). *Acta Geographica Sinica*, 58, 569–576.
- Hakim, G.J., Emile-Geay, J., Steig, E.J., Noone, D., Anderson, D.M., Tardif, R., Steiger, N. and Perkins, W.A. (2016) The last millennium climate reanalysis project: Framework and first results. *Journal of Geophysical Research: Atmospheres*, 121, 6745–6764.
- Hu, C., Henderson, G.M., Huang, J., Xie, S., Sun, Y. and Johnson, K.R. (2008) Quantification of Holocene Asian monsoon rainfall from spatially separated cave records. *Earth and Planetary Science Letters*, 266, 221–232.
- Jiang, D. and Tian, Z. (2013) East Asian monsoon change for the 21st century: Results of CMIP3 and CMIP5 models. *Chinese Science Bulletin*, 58, 1427–1435.
- Jiang, D. and Wang, H. (2005) Natural interdecadal weakening of east Asian summer monsoon in the late 20th century. *Chinese Science Bulletin*, 50, 1923–1929.
- Juckles, M.N., Allen, M.R., Briffa, K.R., Esper, J., Hegerl, G.C., Moberg, A., Osborn, T.J. and Weber, S.L. (2007) Millennial temperature reconstruction intercomparison and evaluation. *Climate of the Past*, 3, 591–609.
- Landrum, L., Otto-Bliesner, B.L., Wahl, E.R., Conley, A., Lawrence, P.J., Rosenbloom, N. and Teng, H. (2013) Last millennium climate and its variability in CCSM4. *Journal of Climate*, 26, 1085–1111.
- Lee, K.E. and Park, W. (2015) Initiation of East Asia monsoon failure at the climate transition from the medieval climate anomaly to the little ice age. *Global and Planetary Change*, 128, 83–89.
- LeGrande, A.N. and Schmidt, G.A. (2009) Sources of Holocene variability of oxygen isotopes in paleoclimate archives. *Climate of the Past*, 5, 441–455.
- Li, D., Li, T., Jiang, H., Björck, S., Seidenkrantz, M.-S., Zhao, M., Sha, L. and Knudsen, K.L. (2018) East Asian winter monsoon variations and their links to Arctic Sea ice during the last millennium, inferred from sea surface temperatures in the Okinawa trough. *Paleoceanography and Paleoclimatology*, 33, 61–75.
- Li, J., Dodson, J., Yan, H., Zhang, D.D., Zhang, X., Xu, Q., Lee, H. F., Pei, Q., Cheng, B., Li, C., Ni, J., Sun, A., Lu, F. and Zong, Y. (2017) Quantifying climatic variability in monsoonal northern China over the last 2200 years and its role in driving Chinese dynastic changes. *Quaternary Science Reviews*, 159, 35–46.
- Li, Y. and Morrill, C. (2014) A Holocene east Asian winter monsoon record at the southern edge of the Gobi desert and its comparison with a transient simulation. *Climate Dynamics*, 45, 1219–1234.
- Liu, B., Jin, H., Sun, L., Sun, Z. and Su, Z. (2013) Winter and summer monsoonal evolution in northeastern Qinghai-Tibetan plateau during the Holocene period. *Chemie der Erde*, 148, 194–208.
- Liu, J., Wang, B., Wang, H., Kuang, X. and Ti, R. (2011) Forced response of the east Asian summer rainfall over the past millennium: Results from a coupled model simulation. *Climate Dynamics*, 36, 323–336.
- Liu, J., Chen, J., Zhang, X., Li, Y., Rao, Z. and Chen, F. (2015) Holocene east Asian summer monsoon records in northern China and their inconsistency with Chinese stalagmite $\delta^{18}\text{O}$ records. *Earth-Science Reviews*, 148, 194–208.
- Liu, X., Dong, H., Yang, X., Herzsuh, U., Zhang, E., Stuut, J.-B. W. and Wang, Y. (2009) Late Holocene forcing of the Asian winter and summer monsoon as evidenced by proxy records from the northern Qinghai-Tibetan plateau. *Earth and Planetary Science Letters*, 280, 276–284.
- Man, W. and Zhou, T. (2014) Regional-scale surface air temperature and east Asian summer monsoon changes during the last millennium simulated by the FGOALS-gl climate system model. *Advances in Atmospheric Sciences*, 31, 765–778.
- Man, W., Zhou, T. and Jungclaus, J.H. (2012) Simulations of the east Asian summer monsoon during the last millennium with the MPI earth system model. *Journal of Climate*, 25, 7852–7866.
- Mann, M.E. and Jones, P.D. (2003) Global surface temperatures over the past two millennia. *Geophysical Research Letters*, 30, 1820.
- Mann, M.E., Zhang, Z., Rutherford, S., Bradley, R.S., Hughes, M.K., Shindell, D., Ammann, C., Faluvegi, G. and Ni, F. (2009) Global signatures and dynamical origins of the little ice age and medieval climate anomaly. *Science*, 326, 1256–1260.
- PAGES 2k Consortium. (2013) Continental-scale temperature variability during the past two millennia. *Nature Geoscience*, 6, 339–346.
- Park, J., Han, J., Jin, Q., Bahk, J. and Yi, S. (2017) The link between ENSO-like forcing and hydroclimate variability of coastal East Asia during the last millennium. *Scientific Reports*, 7, 8166.
- Peng, Y., Shen, C., Wang, W.-C. and Xu, Y. (2010) Response of summer precipitation over eastern China to large volcanic eruptions. *Journal of Climate*, 23, 818–824.
- Peng, Y., Shen, C., Cheng, H. and Xu, Y. (2014) Modeling of severe persistent droughts over eastern China during the last millennium. *Climate of the Past*, 10, 1079–1091.
- Sagawa, T., Kuwae, M., Tsuruoka, K., Nakamura, Y., Ikehara, M. and Murayama, M. (2014) Solar forcing of centennial-scale east Asian winter monsoon variability in the mid- to late Holocene. *Earth and Planetary Science Letters*, 395, 124–135.
- Sen Gupta, A., Jourdain, N.C., Brown, J.N. and Monselesan, D. (2013) Climate drift in the CMIP5 models. *Journal of Climate*, 26, 8597–8615.
- Shi, J., Yan, Q., Jiang, D., Min, J. and Jiang, Y. (2016a) Precipitation variation over eastern China and arid Central Asia during the past millennium and its possible mechanism: Perspectives from

- PMIP3 experiments. *Journal of Geophysical Research: Atmospheres*, 121, 11989–12004.
- Shi, Z., Xu, T. and Wang, H. (2016b) Sensitivity of Asian climate change to radiative forcing during the last millennium in a multi-model analysis. *Global and Planetary Change*, 139, 195–210.
- Sun, B., Wang, H. and Zhou, B. (2019) Interdecadal variation of the relationship between east Asian water vapor transport and tropical Pacific Sea surface temperatures during January and associated mechanisms. *Journal of Climate*, 32, 7575–7594.
- Tan, L., Cai, Y., An, Z., Edwards, R.L., Cheng, H., Shen, C.-C. and Zhang, H. (2010) Centennial- to decadal-scale monsoon precipitation variability in the semi-humid region, northern China during the last 1860 years: Records from stalagmites in Huangye cave. *The Holocene*, 21, 287–296.
- Taylor, K.E. (2001) Summarizing multiple aspects of model performance in a single diagram. *Geophysical Research Letters*, 106, 7183–7192.
- Tu, L., Zhou, X., Cheng, W., Liu, X., Yang, W. and Wang, Y. (2017) Holocene east Asian winter monsoon changes reconstructed by sensitive grain size of sediments from Chinese coastal seas: A review. *Quaternary International*, 440, 82–90.
- Wang, B., Wu, R. and Fu, X. (2000) Pacific-East Asian teleconnection: How does ENSO affected East Asian climate? *Journal of Climate*, 13, 1517–1536.
- Wang, B., Wu, Z., Li, J., Liu, J., Chang, C.-P., Ding, Y. and Wu, G. (2008) How to measure the strength of the east Asian summer monsoon. *Journal of Climate*, 21, 4449–4463.
- Wang, B., Wu, Z., Chang, C.-P., Liu, J., Li, J. and Zhou, T. (2010) Another look at interannual-to-interdecadal variations of the east Asian winter monsoon: The northern and southern temperature modes. *Journal of Climate*, 23, 1495–1512.
- Wang, L. and Chen, W. (2010) How well do existing indices measure the strength of the east Asian winter monsoon? *Advances in Atmospheric Sciences*, 27, 855–870.
- Wang, L., Li, J., Lu, H., Gu, Z., Rioual, P., Hao, Q., Mackay, A.W., Jiang, W., Cai, B., Xu, B., Han, J. and Chu, G. (2012) The east Asian winter monsoon over the last 15,000 years: Its links to high-latitudes and tropical climate systems and complex correlation to the summer monsoon. *Quaternary Science Reviews*, 32, 131–142.
- Wang, Y., Cheng, H., Edwards, R.L., He, Y., Kong, X., An, Z., Wu, J., Kelly, M.J., Dykoski, C.A. and Li, X. (2005) The Holocene Asian monsoon: Links to solar changes and North Atlantic climate. *Science*, 308, 854–857.
- Xiao, S., Li, A., Liu, J.P., Chen, M., Xie, Q., Jiang, F., Li, T., Xiang, R. and Chen, Z. (2006) Coherence between solar activity and the east Asian winter monsoon variability in the past 8000 years from Yangtze River-derived mud in the East China Sea. *Palaeogeography, Palaeoclimatology, Palaeoecology*, 237, 293–304.
- Xie, S.-P., Kosaka, Y., Du, Y., Hu, K., Howdary, J.S. and Huang, G. (2016) Indo-western Pacific Ocean capacitor and coherent climate anomalies in post-ENSO summer: A review. *Advances in Atmospheric Sciences*, 33, 411–432.
- Yamada, K., Kohara, K., Ikehara, M. and Seto, K. (2019) The variations in the east Asian summer monsoon over the past 3 kyrs and the controlling factors. *Scientific Reports*, 9, 5036.
- Yan, H., Sun, L., Oppo, D.W., Wang, Y., Liu, Z., Xie, Z., Liu, X. and Cheng, W. (2011) South China Sea hydrological changes and Pacific Walker circulation variations over the last millennium. *Nature Communications*, 2, 293.
- Yancheva, G., Nowaczyk, N.R., Mingram, J., Dulski, P., Schettler, G., Negendank, J.F.W., Liu, J.Q., Sigman, D.M., Peterson, L.C. and Haug, G.H. (2007) Influence of the intertropical convergence zone on the east Asian monsoon. *Nature*, 445, 74–77.
- Yu, X., Zhou, W., Liu, Z. and Kang, Z. (2011) Different patterns of changes in the Asian summer and winter monsoons on the eastern Tibetan plateau during the Holocene. *The Holocene*, 21, 1031–1036.
- Zhang, P., Cheng, H., Edwards, R.L., Chen, F., Wang, Y., Yang, X., Liu, J., Tan, M., Wang, X., Liu, J., An, C., Dai, Z., Zhou, J., Zhang, D., Jia, J., Jin, L. and Johnson, K.R. (2008) A test of climate, sun, and culture relationships from an 1810-year Chinese cave record. *Science*, 322, 940–942.
- Zhao, M., Li, H.-C., Liu, Z.-H., Mii, H.-S., Sun, H.-L., Shen, C.-C. and Kang, S.-C. (2015) Changes in climate and vegetation of Central Guizhou in Southwest China since the last glacial reflected by stalagmite records from Yelang cave. *Journal of Asian Earth Sciences*, 114, 549–562.

How to cite this article: Yang K, Hua W, Hu Q. A multi-model analysis of the East Asian monsoon changes in the Medieval Climate Anomaly and Little Ice Age. *Int J Climatol*. 2020;40:5084–5097. <https://doi.org/10.1002/joc.6506>